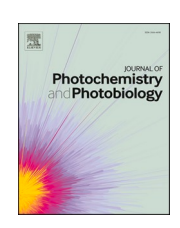
ELSEVIER

Contents lists available at ScienceDirect

# Journal of Photochemistry and Photobiology

journal homepage: www.sciencedirect.com/journal/journal-of-photochemistry-and-photobiology





# Synthesis and Photophysics of Phenylene Based Triplet Donor–Acceptor Dyads: *ortho* vs. *para* Positional Effect on Intramolecular Triplet Energy Transfer

Young Ju Yun<sup>a,b,#</sup>, Manoj K. Manna<sup>a,b,#</sup>, Nareshbabu Kamatham<sup>a,b,#</sup>, Jingbai Li<sup>b</sup>, Shuyang Liu<sup>b</sup>, Francesca Peccati<sup>e</sup>, Barry C. Pemberton<sup>c</sup>, Gary P. Wiederrecht<sup>d</sup>, David J. Gosztola<sup>d</sup>, Gonzalo Jiménez-Osés<sup>e,f</sup>, Andrey Yu Rogachev<sup>b</sup>, A. Jean-Luc Ayitou<sup>a,b,\*</sup>

- <sup>a</sup> Department of Chemistry, University of Illinois at Chicago, Chicago, IL 60607, United States
- b Contribution from Department of Chemistry, Illinois Institute of Technology, Chicago, IL 60616, United States
- <sup>c</sup> School of Natural Sciences and Mathematics, Stockton University, Galloway, NJ, 08205, United States
- <sup>d</sup> Center for Nanoscale Materials, Argonne National Laboratory, Lemont, IL 60439, United States
- e Center for Cooperative Research in Biosciences (CIC bioGUNE), Basque Research and Technology Alliance (BRTA), Bizkaia Technology Park, Building 800, 48160 Derio, Spain
- <sup>f</sup> Ikerbasque, Basque Foundation for Science, 48013 Bilbao, Spain

#### ARTICLE INFO

## Keywords: Triplet photochemistry Triplet energy transfer bichromophores Charge transfer Triplet-triplet annihilation

#### ABSTRACT

Two phenylene based geometrical/isomeric triplet *ortho*- and *para*-dyads (o-3 and p-3, respectively) were synthesized and fully characterized using advanced photophysical tools and computations. In dyad o-3, the through-space donor-acceptor interactions led to simultaneous triplet energy transfer and charge transfer with identical kinetics. On the other hand, in the dyad p-3, it was found that the phenylene spacer favors a fast triplet energy delocalization over the charge transfer process. Furthermore, analysis of the results from the present investigation indicates that the deactivation of the photo-excited species (o-3)\* occurs through both the intrinsic channel viz.  $S_0$ - $S_1$  and charge recombination. In the case of dyad p-3, the results indicate that the primary deactivation pathway is self-quenching or triplet-triplet annihilation involving the acceptor unit(s).

## 1. INTRODUCTION

The efficiency of light-induced triplet energy transfer (TEnT) in organic chromophores is often dictated by the extent of overlap of the interacting chromophores' orbitals (wavefunctions). [1, 2, 3, 4] In this regard, it has been established that molecular interaction(s) in triplet donor/acceptor dyads systems can ultimately influence the resulting efficiency or performance of organic photo-materials and devices that are constructed from these molecular systems. [5, 6] Hence, in order to maximize light-harvesting and triplet energy flow dynamics and/or kinetics within these photo-materials/devices, it is essential to engineer donor-acceptor chromophoric systems that exhibit complementary structural features and/or optoelectronic bandgap. Recent proposals to achieve efficient donor-acceptor TEnT include the use of i) donor and acceptor chromophores with closely related structures, or ii) molecular

templates that link the interacting donor/acceptor chromophores. [7] Capitalizing on the latter approach, chemists have been able to synthesize many triplet bichromophoric systems, which were tailored for applications such as triplet-triplet annihilation based photon upconversion, [8, 9] photocatalysis, [10, 11] bioimaging, [12] and photodynamic therapy. [13, 14, 15, 16, 17, 18, 19]

While the tethering of the donor-acceptor chromophores onto molecular templates is necessary to achieving the ideal photophysical process, this approach may not be sufficient to realize faster TEnT kinetics. In such a design, the through-space or through-bond donor-acceptor triplet energy flow is certainly dependent on the position and orientation of the acceptor chromophores with respect to the triplet energy donor. [7, 20] To elucidate the positional and/or orientational effects on the photo-excited behavior and kinetic of triplet energy flow in organic bichromophores or dyads, we have designed *ortho*-

E-mail address: aayitou@uic.edu (A.J.-L. Ayitou).

<sup>\*</sup> Corresponding Author.

<sup>#</sup> These authors contributed equally

Fig. 1. Chemical structures of ODN (1), perylene (2), dyads o-3 (ortho-dyad 3) and p-3 (para-dyad 3), R = phenyl or n-C<sub>8</sub>H<sub>17</sub>.

and *para*–phenylene dyads using recently reported triplet energy donor and acceptor molecular systems from our group. [21, 22] Previously, we reported that a quinoidal naphthothioamide (QDN) triplet sensitized (1) can be used to sensitize perylene (2) leading to perylene delayed fluorescence via triplet-triplet annihilation. From this prior investigation, it was hypothesized that due to their identical structural features (*viz.* planar backbone), chromophores 1 and 2 would form  $\pi$ - $\pi$  supramolecular solid-solutions. After failing to prepare ideal co-crystalline solid materials using mixtures of chromophores 1 and 2, it became clear to us that the best strategy to create the desired materials is to tether sensitizer 1 and perylene 2 onto a rigid template such as phenylene or triptycene. Following this proposition, we reported recently molecular dyads, where the two chromophores were linked using i) a phenylene spacer which allow *meta*–interaction between the donor and acceptor moieties [23] and ii) a triptycene linker for through-space interaction. [24]

While the *meta*-dyad exhibited similar photophysical features as the parent sensitizer 1, the donor-acceptor interaction in the penylene based dyad produced essentially a charge-transfer (CT) state upon excitation. Herein, we wish to report complementary scenarios with dyads o-3 and p-3 (Figure 1), where it was hypothesized that the ortho- and para--positional effects from the 1/2 interaction could modulate the extent of ground state coupling and excited state triplet energy flow or CT dynamic.

## 2. METHODS

### 2.1. Experimental Section

The synthetic procedures for *ortho/para*–**BrPh**–1 and Bpin–2 and their corresponding precursors are reported in the Supplementary Information (Schemes S1–S8). All spectroscopy measurements were performed using spectroscopy-grade solvents. All NMR characterizations were carried out on a Bruker 300 MHz spectrometer at 298 K. High-resolution mass spectrum data were recorded on a Bruker microTOF II or Shimadzu IT-TOF spectrometers in positive (ESI+) ion mode. UV-vis absorption spectra were recorded on an Ocean Optics spectrometer (DH-MINI UV–vis–NIR light source and QE-Pro detector). Emission spectra were recorded on an Edinburgh Instrument FLS980 spectrometer. Time-resolved pump–probe spectroscopy was performed using an amplified Ti:sapphire laser system (Spectra Physics Spitfire) equipped with an optical parametric amplifier (OPA, Light Conversion, TOPAS). This

system produces 130 fs pulses at 5 kHz centered at 800 nm. 95% of the output from the amplifier is directed to the OPA to generate tunable pump pulses in the visible and near-infrared spectral regions. For operation with 130 fs temporal resolution, the pump pulse and the remaining 5% of output from the amplifier are directed to a transient absorption spectrometer (Helios from Ultrafast Systems), where the 5% output is used to generate a continuum probe pulse extending from 450 nm to 1, 400 nm by focusing into a thin sapphire window. The pump pulse is chopped at half the repetition rate to measure a difference spectrum for the transient absorption measurement. The incident pump pulse for these experiments at 470 nm or 520 nm had energy on the sample of 400 nJ per pulse, focused to a 200-µm-diameter spot. The transmitted probe light was collected and fiber optically coupled to a spectrograph that used a visible (Si) array detector. Data were collected for continuum wavelengths from 450 nm to 750 nm as a function of delay track position for the continuum probe relative to the undelayed pump pulse. The temporal chirp of the data was experimentally determined and corrected before analysis. For longer time scale processes, the probe light comes from a continuum light source (EOS from Ultrafast Systems). In this case, the system operates at 1 kHz and has a time resolution of 200ps/point. Decay times of several hundred microseconds can be measured.

# 2.2. Calculation Details

The geometries of all adducts were optimized with help of hybrid correlation–exchange parameter-free functional of Perdew–Burke–Erzernhof (PBE0). [25, 26] All atoms were described by correlation-consistent basis sets of triple-ζ quality (cc-pVTZ). [27] In all cases, no symmetry restrictions were applied. All these calculations were performed using the Firefly program (version 8.1.0, A. A. Granovsky, Firefly http://classic.chem.msu.su/gran/firefly/index.html)

Using PBEO/cc-pVTZ-optimized geometries, a set of theoretical descriptors/indexes of aromaticity was calculated. This set includes Nuclear Independent Chemical Shift (NICS, introduced by von Rague Schleyer *et al.* [28, 29]), and calculations of NICS values were performed using Gauge Independent Atomic Orbitals (GIAO) approach with help of Gaussian09 program [30] at the PBEO/cc-pVTZ level of theory. Supplementary Information (Tables S1-S4) The set of descriptors was augmented by detailed consideration of magnetic induced ring current on target systems using Anisotropy of the Induced Current Density

**Scheme 1.** Synthesis of phenylene-based donor–acceptor dyad o–3 and p–3. The synthetic procedures of precursors/starting reagents are presented in the Supplementary Information Schemes S1–S8.

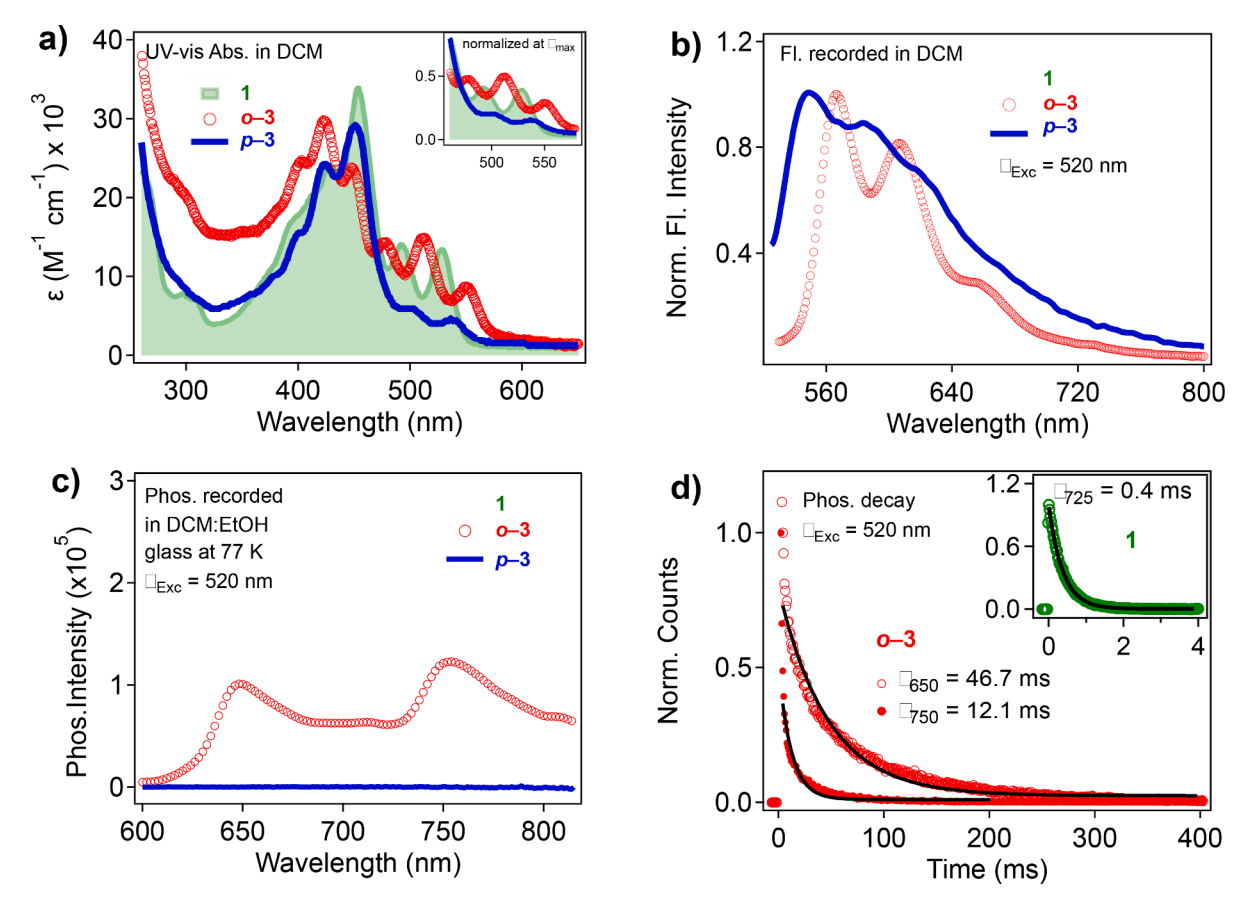


**Fig. 2.** (a) UV-vis absorption spectra of 1 (green), o–3 (red) and p–3 (blue) in DCM; (b) Normalized steady state emission profiles of 1 (green), o–3 (red) and p–3 (blue) in DCM; (c) Time-gated (90 μs delay after pulse) phosphorescence of 1 (green), o–3 (red) and p–3 (blue) in 50:50 (v/v) DCM:EtOH glass at 77 K; (d) Phosphorescence decay kinetics for 1 and o–3 in 50:50 (v/v) DCM:EtOH glass at 77 K at 1 Hz lamp repetition rate: samples O.D. = 0.15 ( $\lambda_{Exc}$  = 520 nm).

(ACID) approach. [31] The applied magnetic field is perpendicular to the five-membered ring. To obtain induced current vectors and plot map, ACID 2.0.0 program uses the current density tensors, calculated by Continuous Set of Gauge Transformations (CSGT) method implemented in Gaussian 09 package. [32] Supplementary Information (Fig. S22)

## 3. SYNTHESIS

Synthesis of dyad o-3: ortho-BrPh-1 (130 mg, 1 equiv., 0.24 mmol) and Bpin-2 (138 mg, 1.5 equiv., 0.36 mmol) were added to a 50 mL toluene and 10 mL EtOH solution. Then, an aqueous solution of  $K_2CO_3$  (3.8 mL (0.5M solution), 8 equiv., 1.94 mmol) was added to the reaction

**Table 1** Optoelectronic parameters of QDN 1 and dyads *o*–3, *p*–3.

Comp.	$\lambda_{Abs}^{\max}$ (nm)	$\epsilon$ (M <sup>-1</sup> cm <sup>-1</sup> ) $^a$	$\lambda_F^{max}$ $(nm)^b$	$\lambda_P^{max}$ $(nm)^b$	$ au_P  ag{ms}^{b,c}$	φ <sub>F</sub> (%)	$\Delta E_{L-H}$ $(eV)^d$
1	454	34, 070	552	725	0.4	0.20	$3.18^{e}$
o-3	422	29, 814	566	755	46.7 &	0.67	3.07
					12.1		
p-3	450	29, 184	560	n.d.	n.d.	0.60	3.18

 $<sup>^{\</sup>rm b}$   $^{a,b}$  UV-vis and Fl. were recorded in DCM; Phosphorescence was recorded in 50:50 (v/v) DCM:EtOH glass at 77 K.  $^{b}\lambda_{\rm exc}=520$  nm;  $^{c}$  Phosphorescence decay kinetics.  $^{d}\Delta E_{\rm L-H}=E_{\rm LUMO}-E_{\rm HOMO}$ ; Calculations were performed using geometries optimized at Calculations were performed at the PBE0/cc-pVTZ level of theory.  $^{e}$ The  $\Delta E_{\rm L-H}$  for QDN 1 was taken from Ref 24.

flask. This mixture was degassed by bubbling N  $\rm N_2$  through the solution for 30 min. Next, Pd(PPh<sub>3</sub>)<sub>4</sub> (30 mg, 11 mol%, 0.03 mmol) was added to the reaction flask. The new mixture was purged with a stream of  $\rm N_2$  and the solution was heated at 90°C for 48 h under constant stirring. After, the reaction solution was cooled to room temperature and quenched with 100 mL of brine. The organic phase was extracted with DCM. The combined organic fraction was dried over anh. Na<sub>2</sub>SO<sub>4</sub> and concentrated in vacuo under reduced pressure using rotavap. The crude compound was purified by flash chromatography over silica gel: solvent system (30% DCM-70% Hexanes). The expected compound ( $\it o$ -3) was obtained as a red solid. Yield: 33 mg, 17%. Scheme 1

 $^{1}\mathrm{H}$  NMR (300 MHz, CDCl<sub>3</sub>)  $\delta$  9.35-9.33 (d, J=6 Hz, 2H), 8.90-8.88 (d, J=6 Hz, 2H), 8.50-8.46 (d, J=12 Hz, 2H), 7.87-7.80 (m, 2H), 7.65-

7.63 (m, 2H), 7.52-7.49 (m, 5H), 7.00-6.98 (m, 6H), 4.80-4.77 (t, J=9 Hz, 2H), 2.02-1.98 (m, 2H), 1.38-1.29 (m, 10H), 0.90-0.85 (t, J=15 Hz, 3H).

(The <sup>1</sup>H NMR spectrum can be found in Figures S15).

HRMS (ESI-TOF) m/z  $[M + H]^+$  calcd for  $C_{48}H_{39}N_2S_2^+$  707.2555, found 707.2549.

**Synthesis of dyad** *p***-3**: Dyad *p***-3** was synthesized according to the procedure we developed for *o***-3** starting with *para*-BrPh-1 (150 mg, 1 equiv., 0.28 mmol) and Bpin-2 (160 mg, 1.5 equiv., 0.42 mmol). *p***-3** was isolated as a red solid. Yield: 48 mg, 23%.

 $^{1}$ H NMR (300 MHz, CDCl<sub>3</sub>) δ 9.29-9.20 (m, 2H), 8.30-8.27 (m, 4H), 7.97-7.85 (m, 1H), 7.87-7.85 (m, 1H), 7.77-7.71 (m, 4H), 7.60-7.50 (m, 6H), 7.19-7.17 (m, 2H), 7.10 (s, 1H), 4.85-4.81 (t, J=12 Hz, 2H), 2.08-2.04 (m, 2H), 1.39-1.31 (m, 10H), 0.92-0.87 (t, J=15 Hz, 3H).

(The <sup>1</sup>H NMR spectrum can be found in Firgures S16.)

HRMS (ESI-TOF) m/z  $[M + H]^+$  calcd for  $C_{48}H_{39}N_2S_2^+$  707.2555, found 707.2549.

## 4. RESULTS & DISCUSSION

#### 4.1. UV-vis Absorption and Emission Spectroscopy

As shown in Figure 2a, the UV-vis absorption profiles of o-3 and p-3 exhibit similar and/or combined transitions and vibronic features from both the sensitizer 1 and the acceptor 2 (Supporting Information, Fig. S17). Nevertheless, a distinctive feature in the absorption profiles of these dyads is the seemingly reduced molar absorption at  $\lambda > 470$  nm, especially in the case of p-3 compared to the profiles of 1 and o-3 (Figure 2a: inset). It was hypothesized that this reduction in the absorption profile of p-3 is the result of through-bond electronic coupling between QDN 1 and the perylene unit 2. Certainly, the para-interaction

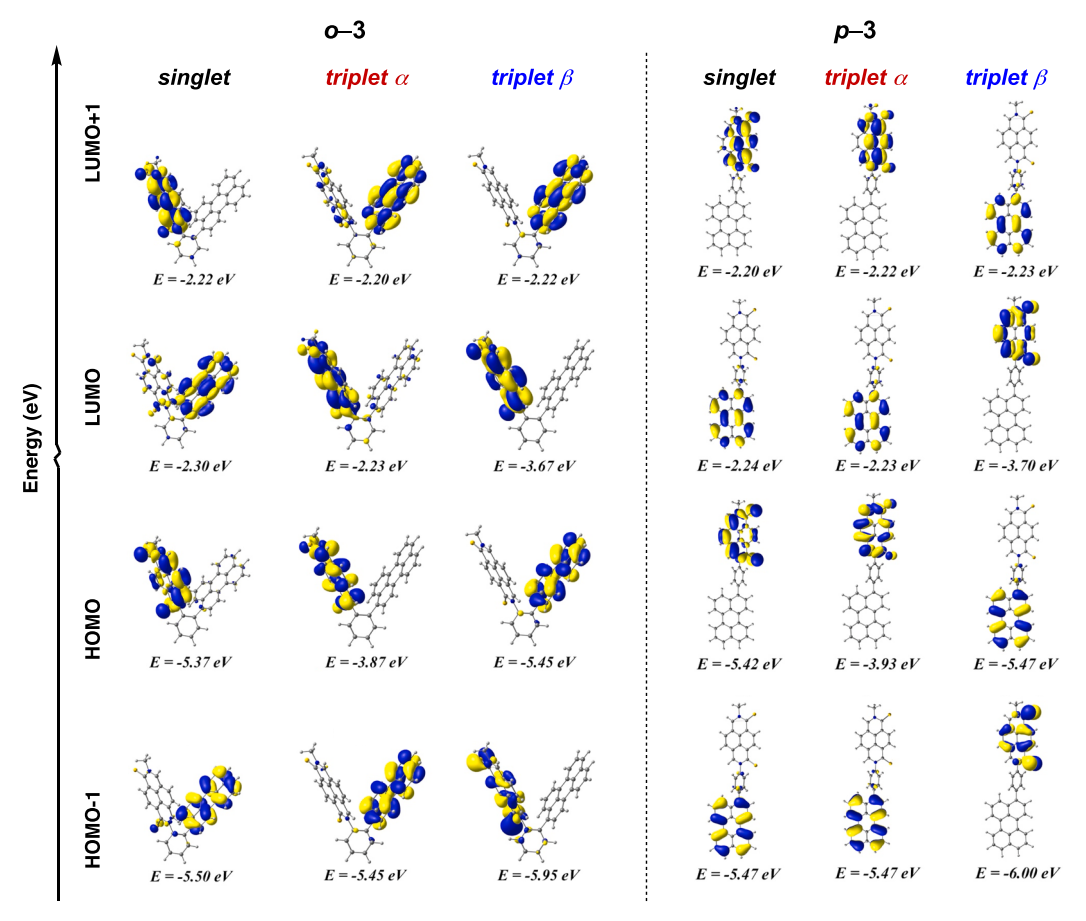
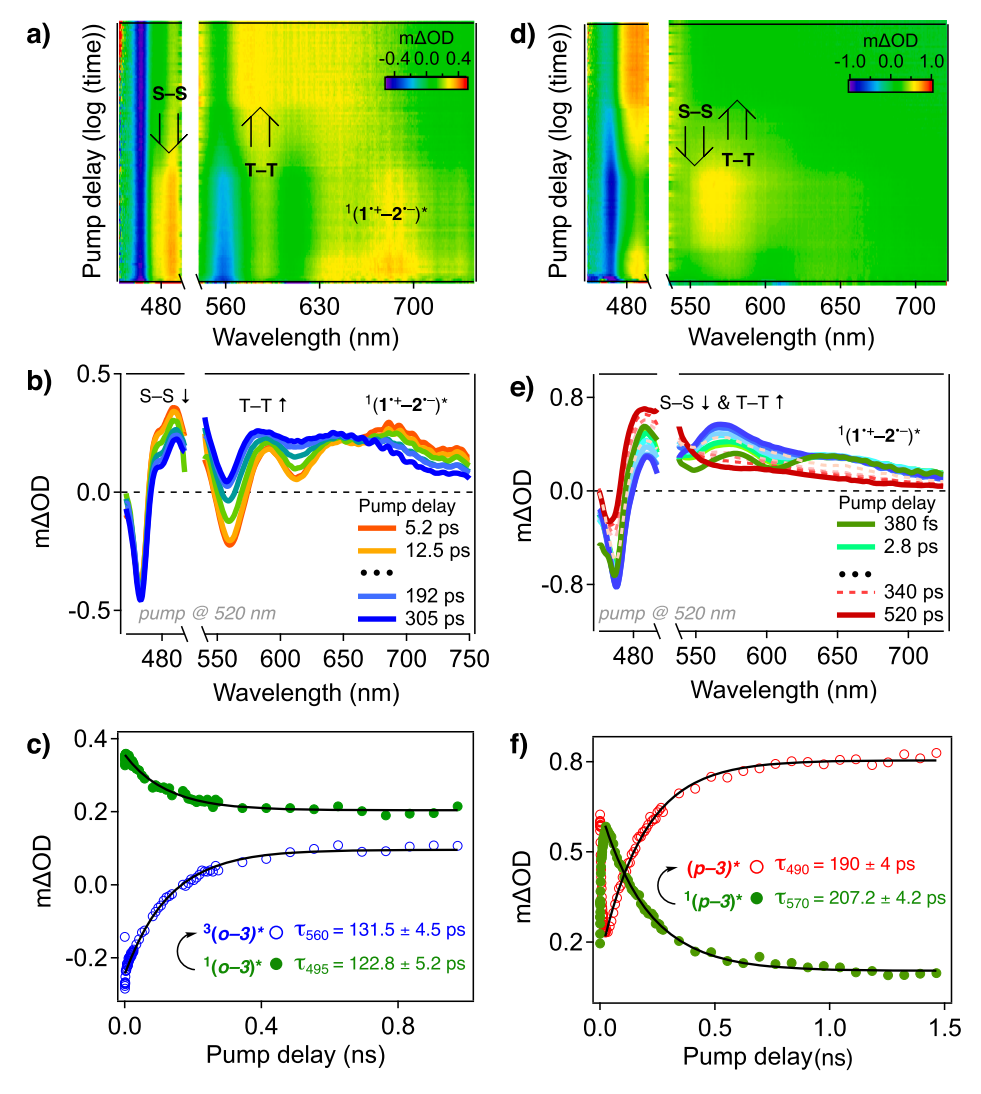


Fig. 3. Frontier molecular orbitals and energies of o-3 and p-3 dyads. Calculations were performed (for R = CH<sub>3</sub>) at PBEO/cc-pVTZ level of theory.

 $<sup>^</sup>c$  Phosphorescence decay kinetics.  $^d$   $\Delta E_{L-H}=E_{LUMO}-E_{HOMO};$  Calculations were performed using geometries optimized at Calculations were performed at the PBE0/cc-pVTZ level of theory.  $^e$  The  $\Delta E_{L-H}$  for QDN 1 was taken from Ref 24.



**Fig. 4.** (a & b) Femtosecond transient absorption map/spectra for o-3 and the corresponding kinetic traces (c); (d & e) Femtosecond transient absorption map/spectra for p-3 and the corresponding kinetic traces (f). Note: Samples for o-3 and p-3 were prepared in oxygen-free THF with optical density O.D. = 0.5 at  $λ_{Exc}$  = 520 nm; laser power = 0.4 μJ/pulse with 2.5 kHz repetition rate.

between QDN 1 and perylene unit 2 could also enhance  $\pi$ -conjugation throughout the whole molecular backbone; hence, the reduced absorption at  $\lambda > 470$  nm is suggestive of "enhanced aromaticity" of the quinoidal ring of chromophore 1, as elaborated in our previous publication. [22] For dyad *o*–3, the absorption profile resembles the one of the parent chromophore 1; but, the appearance of a new transition at ca.  $\lambda = 480$ nm is due energy shifts of the low energy transitions or an intramolecular ground state charge transfer process owing to the close proximity of the interacting chromophores (1 and 2). In this picture, we expected that the intra-dyad interaction 1/2 in the ground state could impact the excited state energy flow dynamics and the associated kinetics. To this end, we first recorded the steady-state emission of o-3 and  $\emph{p}\text{--}3$  (with  $\lambda_{Exc}=520$  nm) and compared the emission profiles to the one of 1. Observation of the emission bands (Figure 2b) of the two dyads indicates that the perylene moiety exerts little effect on the singlet state behavior of the bichromophoric systems. Except the blue-shifted patterns, the fluorescence emission bands of the two dvads show similar vibronic features as seen in the profile of parent donor 1. [22] Furthermore, the broad fluorescence emission band of dyad p-3 indicates the presence of an additional species, presumably from the <sup>1</sup>(CT) \* state.

Interestingly, significant differences were found in the phosphorescence emissions of the two dyads (Figure 2c and 2d). While the emission

band of o-3 is blue-shifted with respect to the one of 1, the triplet state of **p–3** seems quenched, suggesting the following hypotheses: either i) the  $(p-3)^*$  is trapped in the  $(CT)^*$  state (lower in energy than the lowest triplet state), or ii) triplet-triplet annihilation at the perylene moiety is contributing to the quenching of phosphorescence emission. In the two cases, one might expect an additional emission that overlaps with the steady-state radiative decay (Figure 2b). Per this hypothesis, it was concluded that the broad fluorescence emission band from p-3 is suggestive of two overlapped bands: one from  ${}^{1}(p-3)^{*}$  and the other from either the (CT)\* or a delayed emission (vide supra). For dyad o-3, a closer look at the phosphorescence profile (Figure 2c and 2d) reveals various features that can be attributed to the convolution of emission bands from both  ${}^3(1)^*$  and a triplet charge transfer species  ${}^3(1^{\bullet +}-2^{\bullet -})^*$ . With this assumption, we fitted the decay trace of the phosphorescence emission at wavelengths 650 and 750 nm using a mono-exponential function. And the fitting results produced two different lifetime values:  $\tau_{650} = 46.7 \text{ ms}$ and  $\tau_{750} = 12.1$  ms. The smaller lifetime was ascribed to the intrinsic lifetime from the triplet species of the sensitizer 1 within the dyad and the longest lifetime was attributed to the  ${}^{3}(1^{\bullet +}-2^{\bullet -})*$  species. Comparison of the opto-electronic parameters for dyads o-3 and p-3 are summarized in Table 1, where one can see that the increase in  $\Phi_F$  value for the two dyads is suggestive of additional radiative decay, presumably from the (CT)\* state(s).

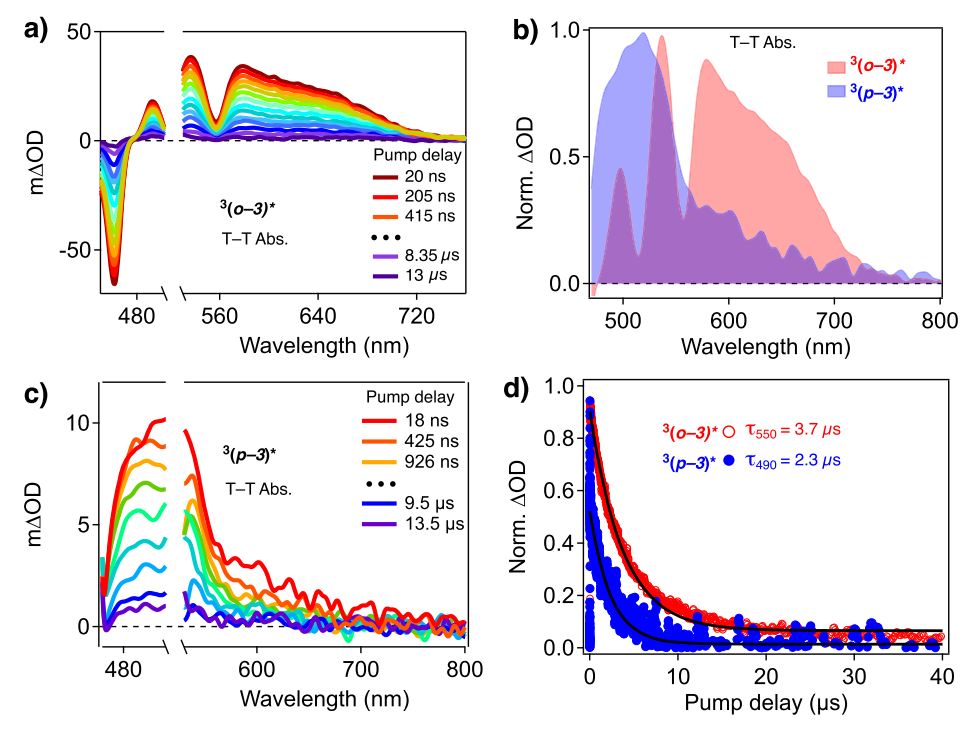
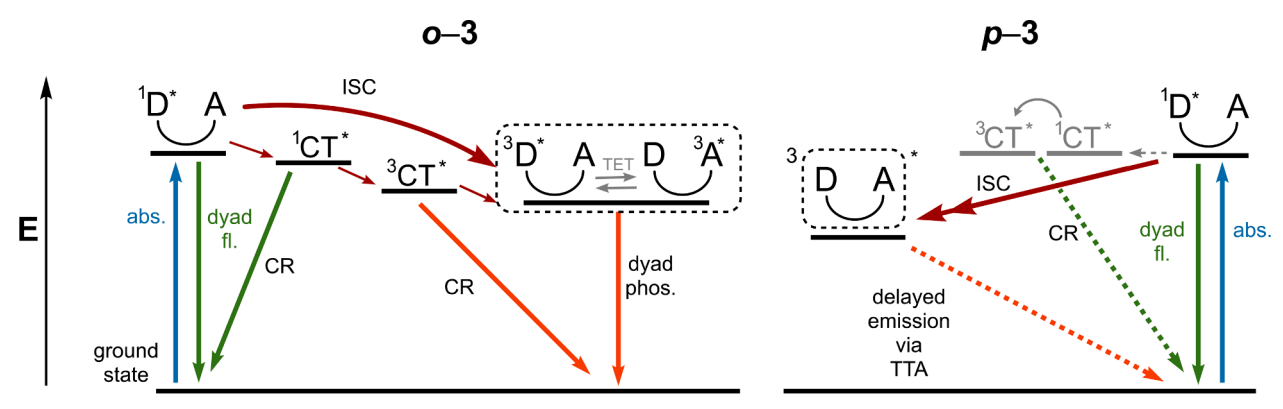


**Fig. 5.** Nanosecond transient absorption spectra for o–3 (a) and p–3 (c); (b) comparison of the transcent spectra at time 18-to-20 ns after the laser pulse; (d) the corresponding normalized decay traces monitored at 550 nm (for o–3) and 490 nm (for p–3). Note: Samples for o–3 and p–3 were prepared in oxygen-free THF with optical density O.D. = 0.5 at λ<sub>Exc</sub> = 520 nm; laser power = 1 μJ/pulse with 1 kHz repetition rate.



ISC = Inter System Crossing | TET = Triplet Energy Transfer | TTA = Triplet-Triplet Annihilation | CT = Charge Transfer | CR = Charge Recombination

Fig. 6. Photophysical pathway of dyads with the proposed deactivation channels upon photo-excitation.: Note: The energy levels of the CT states were positioned hypothetically with respect to the lowest excited states.

## 4.2. Computational Investigations

Next, computational investigations were performed to decipher the extent of electron delocalization across the two dyads. The HOMO and LUMO molecular orbitals of o-3 and p-3 are presented in Figure 3. In the HOMO with singlet multiplicity, the electron density is essentially localized on the QDN moiety only, whereas in the LUMO the electron density is delocalized across the donor and acceptor moieties, indicating probable charge transfer dynamic in the upper-level electronic states. However, between the dyads, the degree of electronic communication between the donor and the acceptor moieties is greater in the case of o-3 than p-3. Thus, it can be concluded that the orientation and position of the individual chromophores in the dyad framework is pivotal to tuning the photo-excited state intra-dyad interactions or the expected triplet energy flow.

It is worth to mention that the nature of the triplet state, as described

in Figure 3, is determined by considering the presence/contribution of the perylene acceptor unit in the molecular skeleton of dyads o-3 and p-3. Also, the results from the calculations revealed that the  $\beta$ -MO is exclusively localized on the acceptor perylene unit (for both systems, o-3 and p-3). This finding is in full agreement with the electronic structure of the neutral systems, specifically with the topology of their LUMOs and also makes a clear bridge to the nature of the corresponding first singlet excited states.

## 4.3. Transient Absorption Spectroscopy

To have a better understanding of the photo-dynamics in the two dyads, we further investigated their corresponding excited state transients and the associated kinetics. Because of the observed dichotomy in the absorption and emission profiles, it was expected that the transient absorptions would also reveal significant differences in photo-behaviors.

In the femtosecond transient absorption spectra for both dyads (Figure 4), the negative absorption at ca. 470 nm is undoubtedly the ground state depletions, which overlap with the UV-vis absorption spectra. For o-3, the positive absorption at ca. 495 nm was ascribed to the singlet transient  ${}^{1}(o-3)^{*}$ , which is quasi-isoenergetic with  ${}^{1}(1^{\bullet+}-2^{\bullet-})$ \* at ca. 700 nm with a decay kinetic of  $\tau_{495/700} = 122.8$  ps. Expectedly, during the decay of the singlet species, a new broad band concomitantly appears at 560-650 nm. The band center at ca. 560 nm has always been assigned to the intrinsic triplet transient <sup>3</sup>(1)\*; [24] however, with the degree of orientation and the short distance separating the donor and acceptor chromophores in this dyad, it can be ascertained that the additional band at ca. 650 nm comes from the formation of the  ${}^{3}(1^{\bullet+}-2^{\bullet-})^{*}$  transient (Figures 4a, b). From the above observations and the earlier hypotheses of the excited state interactions with regard to the proximity of the QDN to the perylene moiety in dyad o-3, we can conclude that the similarity between the temporal decay of the singlet transient and the rise of the triplet transient is facilitated by the CT species  $(1^{\bullet +} - 2^{\bullet -})^*$ .

Unlike o-3, the femtosecond transient spectra of dyad p-3 showed a combination of bands at 480, 560, and 650 nm (Figures 4d, e). However, it is easier to see that the earlier/fast kinetic (green spectrum at 380 fs after laser excitation) encompasses many events viz. pseudo-decay of the  $^1(p-3)^*$  and  $^1(1^{\bullet+}-2^{\bullet-})^*$  and rapid rise of the corresponding  $^3(p-3)^*$  and  $^3(1^{\bullet+}-2^{\bullet-})^*$ . It was not easy to fully deconvolute these events, as these overlap with the instrument-response-time. At longer timescales, all of these transient species seem to co-exist with a decay time constant (at 570 nm) of 207 ps and a time constant of 190 ps for the rise of the band at ca. 490 nm (Figures 4d, e). With these complexities in the photoexcited state of dyad p-3, we hypothesized that although the triplet energy delocalization across the whole dyad is the preferred process/channel, the formation of the  $^3(CT)^*$  species can still occur. But these species will eventually decay via charge recombination.

The nanosecond transient absorption spectra of the two dyads were recorded to monitored the decay of the triplet transients and (CT)\* species. For o-3, since the  $^3(o$ -3)\* transient and the  $^3(1^{o}$ - $(2^{o}$ -)\* form within the same time constant from the singlet transients, it was concluded that the triplet spectrum evokes mixed radiative  $S_0 \leftarrow T_1$  and charge recombination processes with a time constant of 3.7  $\mu$ s. The scenario is different with p-3, where the possibility of triplet energy flow  $(1 \rightarrow 2)$  can lead to the formation of the perylene triplet transient. In this case, we assigned the band centered at ca. 490 nm to perylene triplet-triplet absorption, which a time constant of 2.3  $\mu$ s (Figures 5c, d).

The overlapped triplet-triplet absorption spectra of the two dyads in Figure 5b does corroborate our hypothesis that *ortho*-geometry (in these donor-acceptor chromophoric systems) could lead to both triplet energy flow and charge transfer processes, whereas *para*-geometry favors not only triplet delocalization across the whole molecule, but also the rapid quenching of the triplet at the perylene moiety. The photophysical processes in the two dyads are summarized in Figure 6.

## 5. CONCLUSION

The positional effect on the photo-dynamics in the dyads under study revealed that donor-acceptor interactions can lead to both triplet energy flow and charge transfer processes when the chromophores interact through space in a co-facial manner. On the other hand, when these chromophores interact through the phenylene spacer, the triplet energy flow becomes the predominant process. In dyad o–3, the energy and charge transfer processes occur simultaneously; whereas in dyad p–3, the excited-state dynamic is dominated by triplet energy delocalization donor $\leftrightarrow$ acceptor, which ultimately leads to triplet-triplet quenching at the perylene moiety. Importantly, the photophysical results are in agreement with the computational investigations. The present result provides complementary understanding of geometrical influences on the photophysics of molecular bichromophores, which could be employed for a number of light—harvesting and —modulation processes.

#### **Funding Sources**

National Science Foundation under a CAREER grant no. 1753012 Awarded to AJA.

Illinois Institute of Technology Graduate Kilpatrick and Starr Fieldhouse Fellowships to YJY.

Grant RTI2018-099592-B-C22 from the Agencia Estatal Investigacion of Spain (AEI) to G.J.O.

## ASSOCIATED CONTENT

**Supporting Information**: Details of the synthetic procedures for all precursors of dyads o–3 and p–3:  $^1$ H and  $^{13}$ C NMR spectra, additional UV-vis absorption spectra, emission spectra, IR spectra, and computational data. This material is available free of charge via the Internet at http://elsevier.com.

## **Declaration of Competing Interest**

The authors declare no competing financial interests.

#### ACKNOWLEDGMENT

This material is based upon work supported by the National Science Foundation under a CAREER grant no. 1753012 awarded to AJA. YJY is thankful for the support from the Kilpatrick Graduate Fellowship and the Starr Fieldhouse Research Fellowship Programs at Illinois Tech. GJO thanks the Agencia Estatal Investigacion of Spain for the generous support through the rant RTI2018-099592-B-C22. Use of the Center for Nanoscale Materials, an Office of Science user facility, was supported by the U.S. Department of Energy, Office of Science, Office of Basic Energy Science, under Contract No. AC02-06CH11357.

## Supplementary materials

Supplementary material associated with this article can be found, in the online version, at doi:10.1016/j.jpap.2022.100112.

## REFERENCE

- [1] T.H.T. Thi, C. Desforge, C. Thiec, S. Gaspard, Singlet-singlet and triplet-triplet intramolecular transfer processes in a covalently linked porphyrin-phthalocyanine heterodimer, The Journal of Physical Chemistry 93 (1989) 1226–1233, https://doi. org/10.1021/j.100341a013.
- [2] M.J.G. Peach, D.J. Tozer, Overcoming Low Orbital Overlap and Triplet Instability Problems in TDDFT, The Journal of Physical Chemistry A 116 (2012) 9783–9789, https://doi.org/10.1021/ip308662x.
- [3] J.J. Piet, P.N. Taylor, H.L. Anderson, A. Osuka, J.M. Warman, Excitonic Interactions in the Singlet and Triplet Excited States of Covalently Linked Zinc Porphyrin Dimers, Journal of the American Chemical Society 122 (2000) 1749–1757, https://doi.org/10.1021/ja993241i.
- [4] C. Curutchet, A.A. Voityuk, Environment effects on triplet–triplet energy transfer in DNA, Chemical Physics Letters 512 (2011) 118–122, https://doi.org/10.1016/j. cplett.2011.07.025.
- [5] L. Cao, X. Du, H. Lin, C. Zheng, Z. Chen, S. Tao, Delayed fluorescence materialassisted high performance ternary organic solar cells realized by prolonged exciton lifetime and diffusion length, J Mater Chem C 8 (2020) 17429–17439, https://doi. org/10.1039/d0rc04233a.
- [6] R. Sivakumar, A. Manivel, D. Contreras, M. Paulraj, Carbazole-diazafluorene bipolar fluorophores: Synthesis, thermal stability, optical and electrochemical properties, J Lumin 236 (2021), 118145, https://doi.org/10.1016/j. jlumin.2021.118145.
- [7] G.-J. Huang, M.A. Harris, M.D. Krzyaniak, E.A. Margulies, S.M. Dyar, R. J. Lindquist, Y. Wu, V.V. Roznyatovskiy, Y.-L. Wu, R.M. Young, M.R. Wasielewski, Photoinduced Charge and Energy Transfer within meta and para -Linked Chlorophyll a -Perylene-3, 4:9, 10-bis(dicarboximide) Donor–Acceptor Dyads, J Phys Chem B 120 (2016) 756–765, https://doi.org/10.1021/acs.jpcb.5b10806.
- [8] X. Guo, Y. Liu, Q. Chen, D. Zhao, Y. Ma, New Bichromophoric Triplet Photosensitizer Designs and Their Application in Triplet-Triplet Annihilation Upconversion, Advanced Optical Materials 6 (2018), 1700981, https://doi.org/ 10.1002/adom.201700981.
- [9] Q. Chen, Y. Liu, X. Guo, J. Peng, S. Garakyaraghi, C.M. Papa, F.N. Castellano, D. Zhao, Y. Ma, Energy Transfer Dynamics in Triplet—Triplet Annihilation Upconversion Using a Bichromophoric Heavy-Atom-Free Sensitizer, The Journal of

- Physical Chemistry A 122 (2018) 6673–6682, https://doi.org/10.1021/acs.inca.8b05901
- [10] S. Guo, L. Ma, J. Zhao, B. Küçüköz, A. Karatay, M. Hayvali, H.G. Yaglioglu, A. Elmali, BODIPY triads triplet photosensitizers enhanced with intramolecular resonance energy transfer (RET): broadband visible light absorption and application in photooxidation, Chem Sci 5 (2013) 489–500, https://doi.org/ 10.1039/c3sc52323c.
- [11] L. Ma, W.-H. Fang, L. Shen, X. Chen, Regulatory Mechanism and Kinetic Assessment of Energy Transfer Catalysis Mediated by Visible Light, Acs Catal 9 (2019) 3672–3684, https://doi.org/10.1021/acscatal.9b00146.
- [12] C.H. Mak, R. Liu, X. Han, Y. Tang, X. Zou, H. Shen, Y. Meng, G. Zou, H. Hsu, Thermally Activated Delayed Phosphorescence and Interchromophore Exciton Coupling in a Platinum-Based Organometallic Emitter, Adv Opt Mater 8 (2020), https://doi.org/10.1002/adom.202001023.
- [13] V. Nguyen, Y. Yim, S. Kim, B. Ryu, K.M.K. Swamy, G. Kim, N. Kwon, C. Kim, S. Park, J. Yoon, Molecular Design of Highly Efficient Heavy-Atom-Free Triplet BODIPY Derivatives for Photodynamic Therapy and Bioimaging, Angew Chem-Ger Edit 132 (2020) 9042–9047, https://doi.org/10.1002/ange.202002843.
- [14] S. Swaminathan, C. Fowley, E.R. Thapaliya, B. McCaughan, S. Tang, A. Fraix, B. Captain, S. Sortino, J.F. Callan, F.M. Raymo, Supramolecular nanoreactors for intracellular singlet-oxygen sensitization, Nanoscale 7 (2015) 14071–14079, https://doi.org/10.1039/c5nr02672e.
- [15] Z. Yang, Z. Zhang, Y. Sun, Z. Lei, D. Wang, H. Ma, B.Z. Tang, Incorporating spin-orbit coupling promoted functional group into an enhanced electron D-A system: A useful designing concept for fabricating efficient photosensitizer and imaging-guided photodynamic therapy, Biomaterials 275 (2021), 120934, https://doi.org/10.1016/j.biomaterials.2021.120934.
- [16] J. Jiang, Y. Qian, Z. Xu, Z. Lv, P. Tao, M. Xie, S. Liu, W. Huang, Q. Zhao, Enhancing singlet oxygen generation in semiconducting polymer nanoparticles through fluorescence resonance energy transfer for tumor treatment, Chem Sci 10 (2019) 5085–5094, https://doi.org/10.1039/c8sc05501g.
- [17] A. Bartczak, Y. Namiki, D.-J. Qian, J. Miyake, A. Boguta, J. Goc, J. Łukasiewicz, D. Frąckowiak, The interactions between tetrapyridyl porphyrin and viologen units covalently linked to polymers, J Photochem Photobiology Chem 159 (2003) 259–272, https://doi.org/10.1016/s1010-6030(03)00190-4.
- [18] X.-F. Zhang, N. Feng, Attaching naphthalene derivatives onto BODIPY for generating excited triplet state and singlet oxygen: Tuning PET-based photosensitizer by electron donors, Spectrochimica Acta Part Mol Biomol Spectrosc 189 (2018) 13–21, https://doi.org/10.1016/j.saa.2017.08.005.
- [19] J. Chen, K. Wen, H. Chen, S. Jiang, X. Wu, L. Lv, A. Peng, S. Zhang, H. Huang, Achieving High-Performance Photothermal and Photodynamic Effects upon Combining D–A Structure and Nonplanar Conformation, Small 16 (2020), e2000909. https://doi.org/10.1002/smll.202000909.
- [20] S. Liu, X. Wang, H. Liu, L. Shen, D. Zhao, X. Li, Enhancing triplet sensitization ability of donor-acceptor dyads via intramolecular triplet energy transfer, J Mater Chem C 8 (2020) 3536–3544, https://doi.org/10.1039/c9tc06337d.
- [21] S. Shokri, G.P. Wiederrecht, D.J. Gosztola, A.J.-L. Ayitou, Photon Upconversion Using Baird-Type (Anti)Aromatic Quinoidal Naphthalene Derivative as a

- Sensitizer, The Journal of Physical Chemistry C 121 (2017) 23377–23382, https://doi.org/10.1021/acs.jpcc.7b08373.
- [22] S. Shokri, J. Li, M.K. Manna, G.P. Wiederrecht, D.J. Gosztola, A. Ugrinov, S. Jockusch, A.Y. Rogachev, A.J.-L. Ayitou, A Naphtho-p-quinodimethane Exhibiting Baird's (Anti)Aromaticity, Broken Symmetry, and Attractive Photoluminescence, J Org Chem 82 (2017) 10167–10173, https://doi.org/ 10.1021/acs.joc.7b01647.
- [23] M.K. Manna, S. Shokri, G.P. Wiederrecht, D.J. Gosztola, A.J.-L. Ayitou, New perspectives for triplet-triplet annihilation based photon upconversion using allorganic energy donor & acceptor chromophores, Chem. Commun. 54 (2018) 5809–5818, https://doi.org/10.1039/c8cc01553h.
- [24] Y.J. Yun, N. Kamatham, M.K. Manna, J. Li, S. Liu, G.P. Wiederrecht, D.J. Gosztola, B.T. Diroll, A.Y. Rogachev, A.J.-L. Ayitou, Interplay between Energy and Charge Transfers in a Polyaromatic Triplet Donor–Acceptor Dyad, J Phys Chem C 124 (2020) 12205–12212. https://doi.org/10.1021/acs.ipcc.0c01530.
- [25] J.P. Perdew, K. Burke, M. Ernzerhof, Generalized Gradient Approximation Made Simple [Phys. Rev. Lett. 77, 3865 (1996)], Phys Rev Lett. 78 (1997) 1396, https://doi.org/10.1103/physrevlett.78.1396.
- [26] J.P. Perdew, K. Burke, M. Ernzerhof, Generalized Gradient Approximation Made Simple, Phys Rev Lett 77 (1996) 3865–3868, https://doi.org/10.1103/ physrevlett.77.3865.
- [27] D.E. Woon, T.H. Dunning, Gaussian basis sets for use in correlated molecular calculations. III. The atoms aluminum through argon, J Chem Phys 98 (1993) 1358–1371, https://doi.org/10.1063/1.464303.
- [28] P. von R. Schleyer, C. Maerker, A. Dransfeld, H. Jiao, N.J.R. van E. Hommes, Nucleus-Independent Chemical Shifts: A Simple and Efficient Aromaticity Probe, J Am Chem Soc 118 (1996) 6317–6318, https://doi.org/10.1021/ja960582d.
- [29] Z. Chen, C.S. Wannere, C. Corminboeuf, R. Puchta, P. von, R. Schleyer, Nucleus-Independent Chemical Shifts (NICS) as an Aromaticity Criterion, Chem Rev 105 (2005) 3842–3888, https://doi.org/10.1021/cr030088+.
- [30] M.J. Frisch, G.W. Trucks, H.B. Schlegel, G.E. Scuseria, M.A. Robb, J.R. Hasegawa, M. Ishida, T. Nakajima, Y. Honda, O. Kitao, H. Nakai, T. Vreven, J.A. Montgomery, Jr., J.E. Peralta, Hratchian, A.F. Izmaylov, J. Bloino, G. Zheng, J.L. Sonnenberg, M. Hada, M. Ehara, K. Toyota, R. Fukuda, J.F. Ogliaro, M. Bearpark, J.J. Heyd, E. Brothers, K.N. Kudin, V.N. Staroverov, R. Kobayashi, J. Normand, K. Raghavachari, A. Rendell, J.C. Burant, S.S. Iyengar, J. Tomasi, M. Cossi, N. Rega, J.M. Millam, M. Klene, J.E. Knox, J.B. Cross, V. Bakken, C. Adamo, J. Jaramillo, R. Gomperts, R.E. Stratmann, O. Yazyev, A.J. Austin, R. Cammi, C. Pomelli, J.W. Ochterski, R.L. Martin, K. Morokuma, V.G. Zakrzewski, G.A. Voth, P. Salvador, J.J. Dannenberg, S. Dapprich, A.D. Daniels, Ö. Farkas, J.B. Foresman, J.V. Ortiz, J. Cioslowski, and D.J. Fox, Gaussian 09, Revision D.01, 1989.
- [31] R. Herges, D. Geuenich, Delocalization of Electrons in Molecules †, J Phys Chem 105 (2001) 3214–3220, https://doi.org/10.1021/jp0034426.
- [32] T.A. Keith, R.F.W. Bader, Calculation of magnetic response properties using a continuous set of gauge transformations, Chem Phys Lett 210 (1993) 223–231, https://doi.org/10.1016/0009-2614(93)89127-4.